FEBS Open Bio 4 (2014) 377–386

FEBS openbio

journal homepage: www.elsevier.com/locate/febsopenbio

Fructose 1-phosphate is the one and only physiological effector of the Cra (FruR) regulator of *Pseudomonas putida*

Max Chavarría [a,b], Gonzalo Durante-Rodríguez [a], Tino Krell [c], César Santiago [d], Jan Brezovsky [e], Jiri Damborsky [e], Víctor de Lorenzo [a,*]

[a] *Systems and Synthetic Biology Program, Centro Nacional de Biotecnología (CNB-CSIC), Cantoblanco, Madrid 28049, Spain*
[b] *Escuela de Química, Universidad de Costa Rica, 2060 San José, Costa Rica*
[c] *Department of Environmental Protection, Estación Experimental del Zaidín, CSIC, C/Profesor Albareda, Granada, Spain*
[d] *X-ray Crystallography Unit, Centro Nacional de Biotecnología (CNB-CSIC), Cantoblanco, Madrid 28049, Spain*
[e] *Loschmidt Laboratories, Department of Experimental Biology and Research Centre for Toxic Compounds in the Environment (RECETOX), Faculty of Science, Masaryk University, Kamenice 5/A13, 625 00 Brno, Czech Republic*

ARTICLE INFO

Article history:
Received 14 March 2014
Revised 31 March 2014
Accepted 31 March 2014

Keywords:
Cra
FruR
Pseudomonas putida
Fructose 1-phosphate
Fructose operon

ABSTRACT

Fructose-1-phosphate (F1P) is the preferred effector of the catabolite repressor/activator (Cra) protein of the soil bacterium *Pseudomonas putida* but its ability to bind other metabolic intermediates *in vivo* is unclear. The Cra protein of this microorganism (Cra^{PP}) was submitted to mobility shift assays with target DNA sequences (the P_{fruB} promoter) and candidate effectors fructose-1,6-bisphosphate (FBP), glucose 6-phosphate (G6P), and fructose-6-phosphate (F6P). 1 mM F1P was sufficient to release most of the Cra protein from its operators but more than 10 mM of FBP or G6P was required to free the same complex. However, isothermal titration microcalorimetry failed to expose any specific interaction between Cra^{PP} and FBP or G6P. To solve this paradox, transcriptional activity of a P_{fruB}-*lacZ* fusion was measured in wild-type and Δ*fruB* cells growing on substrates that change the intracellular concentrations of F1P and FBP. The data indicated that P_{fruB} activity was stimulated by fructose but not by glucose or succinate. This suggested that Cra^{PP} represses expression *in vivo* of the cognate *fruBKA* operon in a fashion dependent just on F1P, ruling out any other physiological effector. Molecular docking and dynamic simulations of the Cra-agonist interaction indicated that both metabolites can bind the repressor, but the breach in the relative affinity of Cra^{PP} for F1P *vs* FBP is three orders of magnitude larger than the equivalent distance in the *Escherichia coli* protein. This assigns the Cra protein of *P. putida* the sole role of transducing the presence of fructose in the medium into a variety of direct and indirect physiological responses.

1. Introduction

The enterobacterial catabolite repressor/activator (Cra) protein is a pleiotropic regulator that controls expression of a large number of metabolic genes in response to the flux of central glycolytic intermediates [1,2]. In particular, the Cra protein of *Escherichia coli* (Cra^{EC}) represses transcription of genes such as *fruB*, *pfkA*, *pykA*, *pykF*, *acnB*, *edd*, *eda*, *mtlADR* and *gapB* [1,3–6] while stimulating expression of others e.g., *ppsA*, *fbp*, *pckA*, *acnA*, *icd*, *aceA*, and *aceB* [1,7–10]. The Cra protein was first identified as repressor of the fructose operon (*fruBKA*; [11]) thereby the earlier (and synonymous) name FruR. But, which is the metabolite sensed by Cra, the levels of which report on the status of carbon metabolic fluxes?

The first hints to answer this question came from a number of studies published in the 90s demonstrating that the effects of Cra on transcription can be counteracted *in vitro* by μM levels of fructose-1-phosphate (F1P) as well as by concentrations of fructose-1,6-bisphosphate (FBP) above 5 mM [1,4,11,12]. However, the response of Cra^{EC} to high levels of FBP has been a matter of controversy in the literature, as some studies have suggested that *in vitro* assays of the regulator to this effector could be misleading due to contamination with F1P [11]. In contrast, other Authors claim that FBP is a genuine Cra^{EC} effector [4,13] and that the glycolytic flux of

Abbreviations: Cra, catabolic repression/activation protein; F1P, fructose-1-phosphate; FBP, fructose-1,6-bisphosphate; G6P, glucose 6-phosphate; F6P, fructose-6-phosphate; ITC, isothermal calorimetry

* Corresponding author. Address: Centro Nacional de Biotecnología – CSIC, Campus de Cantoblanco, Madrid 28049, Spain. Tel.: +34 91 585 4536; fax: + 34 91 585 4506.

E-mail address: vdlorenzo@cnb.csic.es (V. de Lorenzo).

http://dx.doi.org/10.1016/j.fob.2014.03.013
2211-5463/

E. coli is sensed by the interaction of the Cra^{EC} with FBP independently of the carbon source used [13,14]. However, the functions of Cra in other species are less clear, as the regulator is also present in bacteria that hardly adopt a metabolic regime (i.e., no glycolytic activity) that produces high FBP levels.

The metabolically versatile soil bacterium *Pseudomonas putida* is one of such cases. In one hand, the central biochemical routes generate F1P only when cells grow on fructose (Fig. 1a and Supplementary Fig. S1; [15]). Moreover, as this bacterium lacks phosphofructokinase, FBP can be produced exclusively only either an upward reaction of trioses back to their cognate hexose, or by phosphorylation of fructose 1-P by FruK (Fig. 1a). Structural, biochemical and biophysical studies have revealed that the Cra protein ortholog of *P. putida* strain KT2440 (Cra^{PP}; 74% similarity and 48% identity with the Cra^{EC}; [16]) regulates the *fruBKA* operon (Fig. 1b) encoding the fructose phosphotransferase system PTS^{Fru} [16,17] and also that F1P is its preferred metabolic effector [16]. Specifically, electrophoretic mobility shift assays (EMSA) showed that as little as 1 μM of F1P prevented binding of purified Cra^{PP} to the P_{fruB} promoter DNA. In contrast no effects on the Cra^{PP}-DNA complex were brought about by any other metabolite tested at the concentrations up to 1 mM. Isothermal titration calorimetry (ITC) experiments with the same protein revealed also that F1P binding to Cra^{PP} occurs with a 1:1 stoichiometry and a very high affinity (K_D ~200 nM). But consistently with the EMSA experiments, neither FBP nor glucose-6-phosphate (G6P) generated any ITC signal when mixed with Cra^{PP} [16]. Finally, while diffracting Cra^{PP}-F1P co-crystals are easy to produce, it has not been possible thus far to generate Cra^{PP}-FBP counterparts. Taken together, the data above suggest that there is no interaction of FBP with the Cra^{PP} protein, at least at effector concentrations ⩽1 mM. Still, the literature reports that intracellular pools of FBP and other glycolytic intermediates can go in bacteria up to >15 mM under some physiological conditions [18]. Therefore, the published experiments do not altogether rule out that other compounds can also be physiological effectors of Cra^{PP}.

In view of the uncertainly on the role of FBP as agonist of Cra^{PP} we set out to clarify unequivocally the nature of the metabolic signal that lets this regulator to detach *in vivo* from its genomic binding sites. By using a suite of biochemical, computational and genetic approaches we show that no metabolite other than F1P may act as an effector of Cra^{PP}. Since F1P is generated in *P. putida* exclusively from exogenously added fructose, we argue that Cra^{PP} is the main transducer of the presence of this sugar in the medium into up/down downregulation of a large number of genes, whether directly (i.e., via interaction with genomic Cra^{PP}-binding sites) or indirectly through the action of proteins of the PTS^{Fru} system encoded by *fruBKA*.

2. Results and discussion

2.1. Binding of Cra^{PP} protein to DNA fragments containing single and double operators

The conditions of reference for examining the influence of various glycolytic intermediates in the attachment of Cra^{PP} to its genomic operators [16] is shown in Fig. 2a. The test involves 3 components: the Cra^{PP} protein purified to homogeneity [16], a 290 bp radioactively labeled DNA fragment spanning the single operator for the regulator found in the P_{fruB} promoter (Fig. 1b; [16,17]) and F1P as an effector. Consistently with previous data (i) as little as 50 nM protein suffices to bind 100% of the target

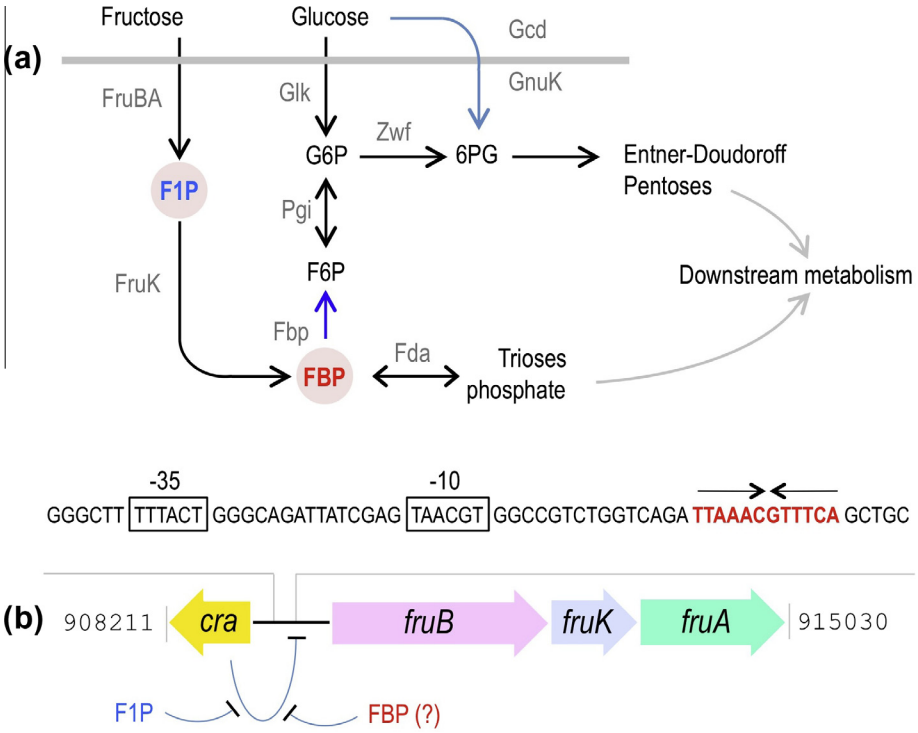

Fig. 1. Metabolic regulation of the fructose operon of *P. putida*. (a) Generation of F1P and FBP upon entry of hexoses in the metabolic network of *P. putida*. F1P is produced from extracellular fructose, which enters the cell through the PTS^{Fru} system (FruBA). FBP is generated also from fructose by phosphorylation of F1P by FruK. When growing on glucose or succinate the lack of phosphofructokinase [15] makes FBP to be produced exclusively through a back reaction of trioses into hexoses. Relevant enzymes and transformations are indicated (see Supplementary Fig. S1 for an expanded metabolic map). (b) Regulatory region of the *fruBKA* operon of *P. putida*. Note the organization of the genes and the P_{fruB} promoter containing one Cra operator (the quasi-palindromic 5′TTAAACGTTTCA3′ sequence in red). While F1P de-represses the promoter by releasing Cra binding to P_{fruB}, the role of FBP is less clear. Numbers flanking the operon indicate the genomic coordinates of the *fruR fruBKA* operon of *P. putida* KT2440.

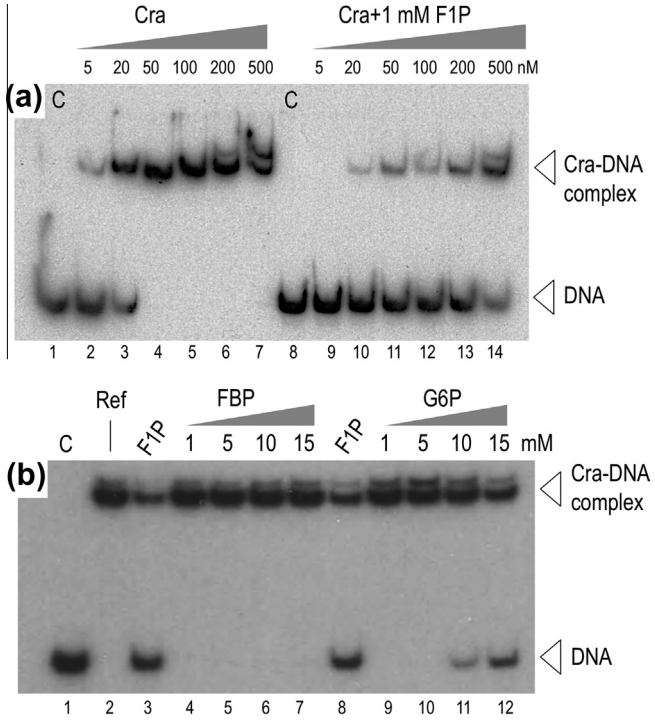

Fig. 2. Interactions of the Cra protein of *P. putida* with its target region of the fructose operon in response to various metabolic effectors. (a) Retardation assay with increasing concentrations of Cra in the absence or presence of F1P 1 mM. Lane 1: Control free DNA probe containing the P_{fruB} promoter of *P. putida*, which has one single Cra operator (Fig. 1b). Lanes 2–7: 5 to 500 nM of Cra protein-only, no effector. Lane 8: DNA probe in the presence of 1 mM F1P, no protein (control, C). Lanes 9–14: 5 to 500 nM of Cra protein with 1 mM F1P. (b) Retardation assay with 50 nM of Cra and different candidate effectors. Lane 1: free DNA probe, no protein (control, C). Lane 2: 50 nM Cra only, no effectors (Ref). Lane 3: 50 nM Cra protein and 1 mM F1P. Lanes 4–7: 50 nM Cra protein and 1–15 mM FBP. Lane 8: 50 nM Cra protein and 1 mM F1P. Lanes 9–12: 50 nM Cra protein 50 nM and 1–15 mM of G6P. Gel experiments were performed as indicated in the Section 4.

DNA (K_D = 26.3 ± 3.1 nM; [16]) and (ii) the presence of F1P releases most of the DNA-Cra^{PP} complex and impedes such a complete binding to occur *in vitro*, even at the highest concentrations of the regulator. The data of Fig. 2a is also consistent with the binding to one single-site operator, as present in the DNA probe employed, at least through Cra^{PP} levels 5–500 nM. Given the extraordinary sensitivity of the EMSA test, we used the same setup for examining the potential of other glycolytic intermediates i.e., FBP and G6P to act also as agonists of the same regulator. To this end we repeated the conditions of the experiment of Fig. 2a but using mM concentrations of each of the candidate effectors. Note that the binding mixtures contain 50 nM of purified His$_6$-Cra^{PP} [16], 0.05 nM of the labeled DNA fragment and 1–15 mM of each potential agonist (Fig. 2b). Therefore the effectors are in large molar excess, up to 3×10^5-fold. The gel of Fig. 2b shows that while FBP had no detectable effect on the stability of the Cra^{PP}-DNA interaction, G6P was able to partially dissociate the complex at its highest concentrations i.e., ⩾10–15 mM. A third glycolytic intermediate, fructose-6-P (F6P) was tested as well, but we did not observe any effect in the stability of the Cra^{PP}-DNA interaction even when added to the binding reaction at the highest concentration (not shown).

Although the results of Fig. 2 were observed at very high effector levels, they do open the possibility that F1P could not be the only Cra^{PP} agonist. Since increasing further the concentrations of Cra^{PP}, FBP or G6P in the assays for verifying such a possible outcome would make little physiological sense we resorted to a different strategy for amplifying the sensitivity of the binding assay. To this end, we employed a DNA sequence containing two operators for Cra instead of the one used before. The rationale of this choice is that one can expand the effector sensitivity of a regulatory device by changing the affinity of the cognate transcription factor (TF) for DNA rather than altering the effector-protein interaction proper. In this way, a residual responsiveness of the TF to an effector becomes well detectable if the affinity for the target operator is artificially enhanced [19]. In our case, the alternative probe is a 290 bp DNA fragment corresponding to the regulatory region of fructose operon of *E. coli* (Supplementary Fig. S2) which is known to contain two site (O_1 5′TGAAACGTTTCA3′; O_2 5′TGAA TCGTTTCA3′) that are cooperatively bound by the regulator [11]. Fig. 3a shows how the Cra^{PP} protein interacts with such a target DNA with two binding sites and the disrupting effect of adding F1P. The two retarded bands that show in the gel are explained as the result of Cra^{PP} binding to either one (complex I) or both operators (complex II) in the labeled DNA probe. When the EMSAs were repeated with high FBP and G6P concentrations (Fig. 3b), the results indicated much more clearly than in the case of the single-operator probe (cf. Fig. 2b) that both glycolytic intermediates could revert the protein-DNA interactions. These results are compatible with earlier observations by Ramseier et al. [11] in that the transcriptional repression caused by Cra^{EC} can be relieved *in vitro* by ⩾5 mM FBP. Still, as these effector concentrations are at the upper limit and beyond those reported in the literature [18] there is a legitimate doubt of whether the action of FBP on Cra^{PP} binding to DNA reflects a genuine, specific regulatory occurrence. Alternatively, they could be the result of using artifactually high effector concentrations that lead to non-reliable effects. The *in vitro* and *in vivo* experiments below were designed to shed light on this outstanding question.

2.2. Interactions of Cra^{PP} with FBP and G6P are unspecific

In order to shed light on the nature of Cra effector(s), the interaction parameters of purified Cra^{PP} with the two principal candidate metabolites were examined by means of isothermal titration microcalorimetry (ITC) as explained in the Methods section. The benchmark for these tests was the ITC signals brought about by the interaction of the same Cra^{PP} used in the EMSA experiments with the *bona fide* effector F1P. Prior to microcalorimetric assays of the protein a number of buffer titrations were carried out to identify the maximal concentration of a compound that give rise to acceptable dilution heats. For the compounds studied, such concentration was found to be 1 mM. The reference titration of Cra with F1P under such conditions is shown in Fig. 4b (equivalent to ITC curve I in Fig. 4c). This control reproduced faithfully the results reported in [16]: F1P binding to Cra^{PP} caused favourable enthalpy changes, the effector-protein complex had an apparent stoichiometry of one F1P/monomer, and the K_D ~200 nM. When this experiment was repeated with FBP or G6P heat changes were identical to the buffer titration with this ligand, indicating an absence of binding (curves I of Fig. 4a and b). Note that under the experimental conditions used the final ligand concentration in the cell was of 175 μM, which implies that a low-affinity interaction cannot be detected. Increasing the concentration of the ligand was not possible due to large dilution heats at the concentrations above 1 mM for all metabolites studied. To visualize a potential low-affinity interaction between FBP and Cra, an alternative strategy was chosen in which a mixture of 12 μM Cra^{PP} with 5 mM of FBP was titrated with a mixture of 0.45 μM F1P in 5 mM FBP. If FBP bound to Cra with an affinity in the lower mM range, the presence of this ligand at Cra would alter the thermodynamic parameters of F1P as mentioned above (Fig. 4b). However, this was not the case because the titration pattern of the Cra^{PP}-FBP mixture with F1P (curve II in Fig. 4c) revealed thermodynamic parameters close to the titration of Cra^{PP} with F1P-only (ITC curve I

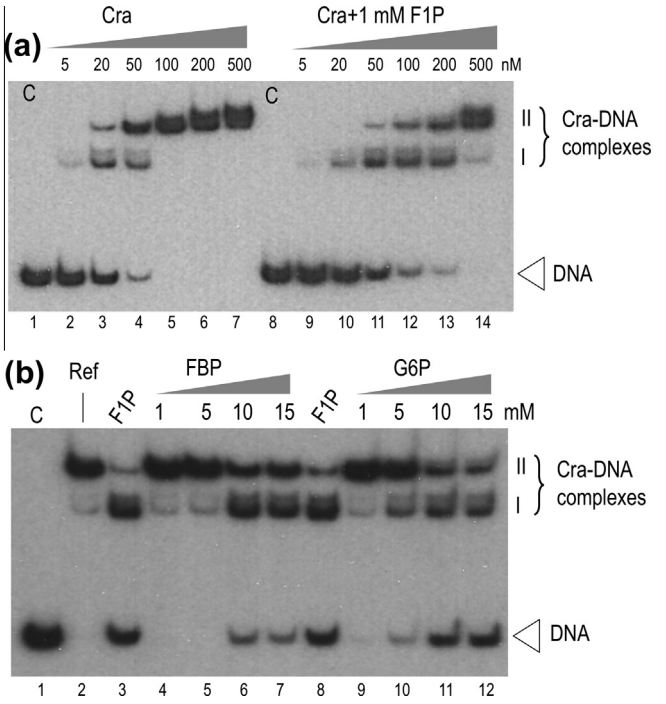

Fig. 3. Binding of the Cra protein of *P. putida* to a target DNA containing two cooperative sites. (a) Retardation assay with increasing concentrations of Cra in the absence or presence of F1P 1 mM. Lane 1: Control free DNA probe containing the P_{fruB} promoter of *E. coli*, which has two cooperative Cra-binding sites (Supplementary Fig. S2). Lanes 2–7: 5 to 500 nM of Cra protein-only, no effector. Lane 8: DNA probe in the presence of 1 mM F1P, no protein (control, C). Lanes 9–14: 5 to 500 nM of Cra protein with 1 mM F1P. (b) Retardation assay with 50 nM of Cra and different candidate effectors. Lane 1: free DNA probe, no protein (control, C). Lane 2: 50 nM Cra only, no effectors (Ref). Lane 3: 50 nM Cra protein and 1 mM F1P. Lanes 4–7: 50 nM Cra protein and 1–15 mM FBP. Lane 8: 50 nM Cra protein and 1 mM F1P. Lanes 9–12: 50 nM Cra protein 50 nM and 1–15 mM of G6P.

in Fig. 4c). These series of ITCs therefore revealed that Cra^{PP} does not bind FBP with affinities in the lower milimolar range, thereby indicating that the protein is highly selective for F1P. These data are not entirely compatible with the evidence of Fig. 3 showing that augmenting the sensitivity of Cra^{PP} binding to its DNA targets allowed to see a clear effect of high concentrations of either FBP or G6P in the stability of the complex. What could be the origin of such a phenomenon? Since we were unable to come to a conclusion with the biochemical approaches described above we resorted to a super-sensitive *in vivo* biosensor system for unequivocally determine the physiological effector(s) of the protein at stake.

2.3. In vivo experiments designate F1P as the only physiological effector of Cra^{PP}

In order to solve the conundrum above (i.e., Cra^{PP} responds to high concentrations of FBP in EMSA experiments but specific interactions are not detected with ITC) we recreated the regulatory system *in vivo* with various genetic constructs. To this end we first transferred the low-copy number plasmid pMCH1 [17] to *P. putida* KT2440. This plasmid carries a translational fusion *fruB′-′lacZ* which allows the readout of Cra^{PP} binding *in vivo* to the promoter of the *fruBKA* operon. In the absence of metabolic effectors, Cra^{PP} binds strongly its operator in the region of the P_{fruB} promoter (Fig. 1) and represses production of β-galactosidase [16,17]. On the contrary, when Cra^{PP} metabolic agonists release repression, the *lacZ* fusion is transcribed and the reporter is expressed. In order to measure accurately β-galactosidase we adopted a variant of the Miller assay [20] that uses the super-sensitive β-Galacto-Light Plus™ luminiscent substrate of the enzyme [21].

Since *P. putida* cannot internalize phosphorylated sugars F1P/FBP, these effectors could not be added directly to the medium for examining their action *in vivo*. Instead, as the metabolic map of *P. putida* KT2440 has been determined ([15,22,23]; Supplementary Fig. S1) we considered to manipulate intracellular levels of F1P or FBP by growing the cells on distinct substrates. Significant concentrations of F1P can be brought about by simply growing cells on fructose, because this hexose becomes transformed instantly into F1P upon transport through the PTS^{Fru} system (Fig. 1a; [17]). However, growth in the same sugar also leads to generation of low-mM concentrations of FBP (~1.3 mM, Fig. 5a), what makes interpretation of any *fruB′-′lacZ* induction result impossible. Therefore, we attempted to increase the concentration of FBP, while keeping F1P levels to the lowest achievable *in vivo*. Analysis of FBP in succinate-grown and glucose-grown cells revealed levels of this effector in the range 60 μM and 275 μM, respectively (Fig. 5a). Since, according to the metabolic models of *P. putida*, F1P can only be generated by fructose (Supplementary Fig. S1), any *fruB′-′lacZ* activity of cells growth on either succinate or glucose should be traced to the effect of FBP. Inspection of the results of Fig. 5b indicated that the *fruB′-′lacZ* was strongly induced as expected in fructose-grown cells and not induced at all in succinate cultures. These extreme values set the upper and the lower limits of activity of the reporter fusion, as there was a plenty of an optimal inducer (F1P, fructose) and very low concentrations of the candidate effector (FBP, succinate). However in the presence of glucose reporter cells nearly tripled the readout of β-galactosidase as compared to succinate conditions (Fig. 5c). Since F1P cannot be formed under these conditions, the result suggested that the levels of FBP detected in these cells could induce the P_{fruB} promoter and thus be an authentic physiological effector of Cra^{PP}. The data shown in Fig. 6, however, ruled out altogether this possibility. In this case, we repeated the same experiment with glucose but using a Δ*fruB* mutant as the host of the *fruB′-′lacZ* reporter system. This strain is unable to transport fructose and therefore cells exclude any possible trace of this sugar that may contaminate the glucose added to the medium. When β-galactosidase was measured in the Δ*fruB* strain, the differences between succinate and glucose altogether disappeared (Fig. 6a). To ensure that the lack of *fruB* entirely prevented the entry of fructose in the medium we run a control experiment in which succinate-grown cells having or lacking a functional *fruB* gene were added with growing concentrations of fructose. As shown in Fig. 6c, as little as 10 μM fructose sufficed multiply by 3-fold the levels of β-galactosidase of succinate-grown wild-type cells. In contrast, the Δ*fruB* mutant kept very low the activity of the reporter even at higher fructose concentrations. Taken together, these results mean that (i) the levels of FBP that *P. putida* cell may accumulate are not sufficient to de-repress the P_{fruB} promoter, (ii) FBP is not a physiological effector of the Cra^{PP} protein and (iii) the residual expression of *fruB′-′lacZ* in glucose-grown cells is due to a contamination of this sugar by traces of fructose. Although the glucose employed in the experiments of Figs. 5 and 6 has the maximum commercial purity (>99.5%, SIGMA), this sugar can be partially converted to fructose in both slightly acid and basic aqueous solutions [24]. The process begins by the spontaneous opening of the hemiacetal ring to an open-chain aldehyde, which undergoes keto-enol tautomerization to its enediol form – which is shared by the two sugars. Subsequent tautomerization to different keto forms produces open-chain fructose, the cyclization of which completes the process. On this basis, it has been calculated that >1% of glucose can tautomerize to fructose [25]. Such traces of fructose would suffice to explain the induction of *fruB′-′lacZ* in glucose-grown cells – while clarifying the conundrum of FBP as a non-agonist of Cra^{PP}. We cannot rule

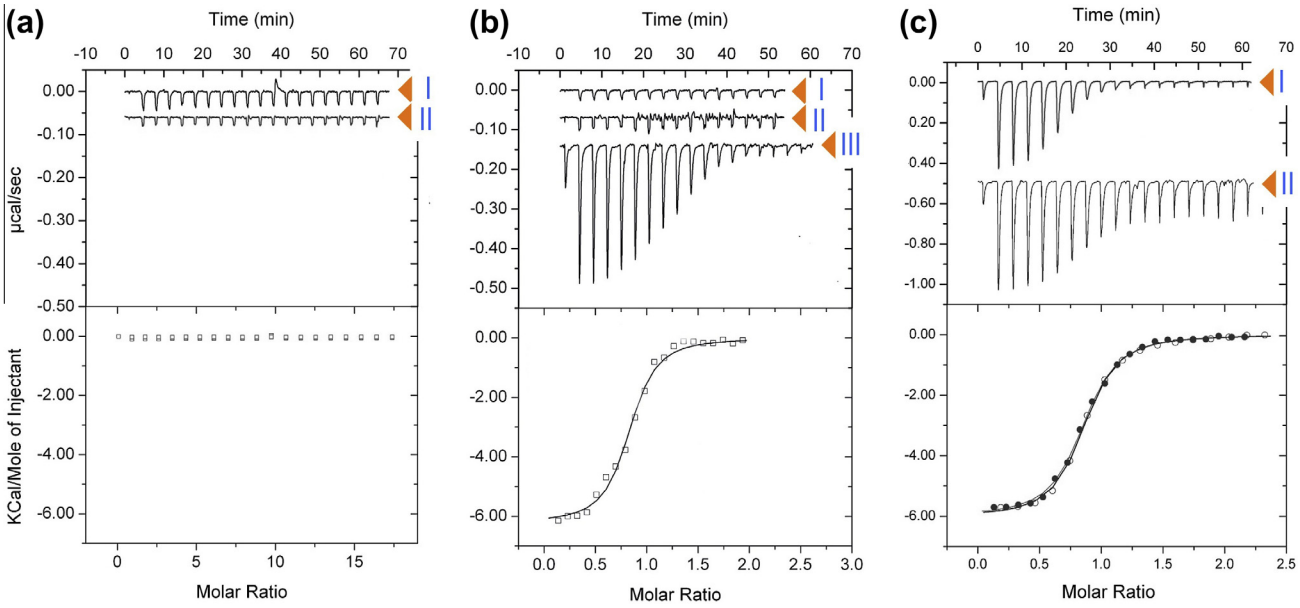

Fig. 4. ITC assays with Cra and effectors. The upper panels plot raw data from representative ITC experiments, whereas the lower panels show the fitted curves of the same results but integrated and corrected for dilution. (a) Titration of dialysis buffer (I) and 12 µM of Cra (II) with 14.4 µl aliquots of 1 mM FBP. (b) Titration of dialysis buffer (I) and 12 µM of Cra (II) with 14.4 µl aliquots of 1 mM G6P. (III) corresponds to positive control. i.e., titration of 12 µM of Cra with 3.2 µl aliquots of 0.5 mM of F1P. (c) ITC competition experiments were performed by titration of 12 µM Cra containing 5 mM FBP with 4.8 µl of a mixture of 0.45 µM F1P and 5 mM FBP (II and filled circles in the bottom panel). The figure also shows the titration of 12 µM Cra with 4.8 µl aliquots of 0.5 mM F1P (I, and empty circles in the bottom panel). The bottom panel corresponds to the superposition of the titration curves of the experiments mentioned above, which are virtually identical, suggesting that FBP does not bind to Cra^{PP}. Note that only the titration with F1P produces a heat change in the experiment at the tested concentrations. Negative peaks are indicative of an exothermic event.

out either that the effect of FBP and G6P on the Cra^{PP} protein *in vitro* (Figs. 2 and 3) could be due to traces of F1P in the corresponding preparations.

The results above on the exclusivity of F1P as the physiological Cra effector raise the issue of their generalization to bacteria other than *P. putida*. While in this species the TF seems to have specialized in controlling fructose uptake, the orthologs in other bacteria (in particular, *E. coli*) have been found to respond to both F1P and FBP and behave as sensors of the glycolytic flux [13]. In order to identify the structural basis for such functional divergence in otherwise very similar proteins, we resorted, to molecular modeling for comparing the interaction details of the Cra^{PP} and its enterobacterial counterpart (i.e., the *E. coli* protein Cra^{EC}) with their effectors F1P and FBP.

2.4. Molecular docking exposes the exclusivity of F1P as the metabolic effector of Cra^{PP}

In order to analyze the binding potential of F1P and FBP to Cra^{PP} we performed separate docking of these metabolites into the X-ray structure of the regulator available in the RSCB PDB database using as a reference the counterpart TF from *E. coli*. Since the crystal structures included the two monomers of the functional protein (chain A and chain B; [16]) the molecular docking was performed separately into either of them (Fig. 7). We first addressed the docking of Cra^{PP} complexed with F1P (PDB: 3O75; [16]), which revealed 19 possible favorable binding modes to the chain A and 20 to the chain B (Supplementary Table S1). For each chain, the predicted binding types that matched experimentally the way of interaction with F1P were found to rank the first and the second by their lowest binding energies and were the most prevalent among all calculated binding modes (40.4% and 37.6%). When the same structure (PDB: 3O75) was tested for FBP binding, the docking identified 26 binding modes to the chain A and 24 to the chain B (Supplementary Table S2). While the simulated binding modes of FBP to either chain ranked the first and the third by their lowest energies, their occurrences (15.2% and 10.4%, respectively) were far less frequent in comparison to F1P. We then explored binding of the same effectors to the effector-free crystal structure of Cra^{PP} (PDB: 3O74; [16]), what resulted in 13 possible binding modes to the chain A and 17 to the chain B (Table S3). The simulations of binding energies in this case ranked very closed to those derived from the 3O75 structure, but the occurrences of each binding mode to effector-free Cra^{PP} were less frequent (8.4% and 7.6% to the chain A and B, respectively), thereby indicating a probable conformational adaptation of Cra induced upon F1P binding. Docking of FBP into the 3O74 structure resulted in 20 possible binding modes to the chain A and 19 to the chain B (Supplementary Table S4). These modes ranked the second and the sixth by their lowest binding energies, but, as above, their occurrences (13.2% to the chain A and 8.4% to the chain B) changed only slightly in comparison with the results obtained for 3O75 structure. Finally, we simulated the binding of F1P and FBP to the effector-free crystal structure of the protein of *E. coli* (PDB: 2IKS, unpublished). In one case, docking of F1P into 2IKS resulted in 47 binding modes to the chain A and 46 to the chain B (Supplementary Table S5), which possessed the seventh and the thirty-first lowest binding energies. The same with FBP yield 73 possible binding modes to the chain A and 58 to the chain B (Supplementary Table S6), ranking the thirty-sixth and the thirty-seventh by their binding energies. Interestingly, the binding occurrences of both F1P (3.2% and 0.4% to the chain A and B) and FBP (0.8% and 0.4%) to Cra^{EC} were quite rare in comparison to Cra^{PP}.

Table 1 shows the overview for the molecular docking results of F1P and FBP into the three different crystal Cra structures averaged over the two polypeptide chains. The data indicate that (i) binding of either effector into the binding site of any of the Cra variants tested is thermodynamically favored and (ii) F1P is always preferred over FBP irrespective of the Cra type. While the difference between the energy released by of F1P and FBP binding to Cra^{PP} was as high as ~2 kcal/mol, the breach decreased by half (~1 kcal/mol) in the case of to Cra^{EC}. This accounts for the extraordinary selectivity of Cra^{PP} for F1P (K_D = 209 ± 20 nM) as compared

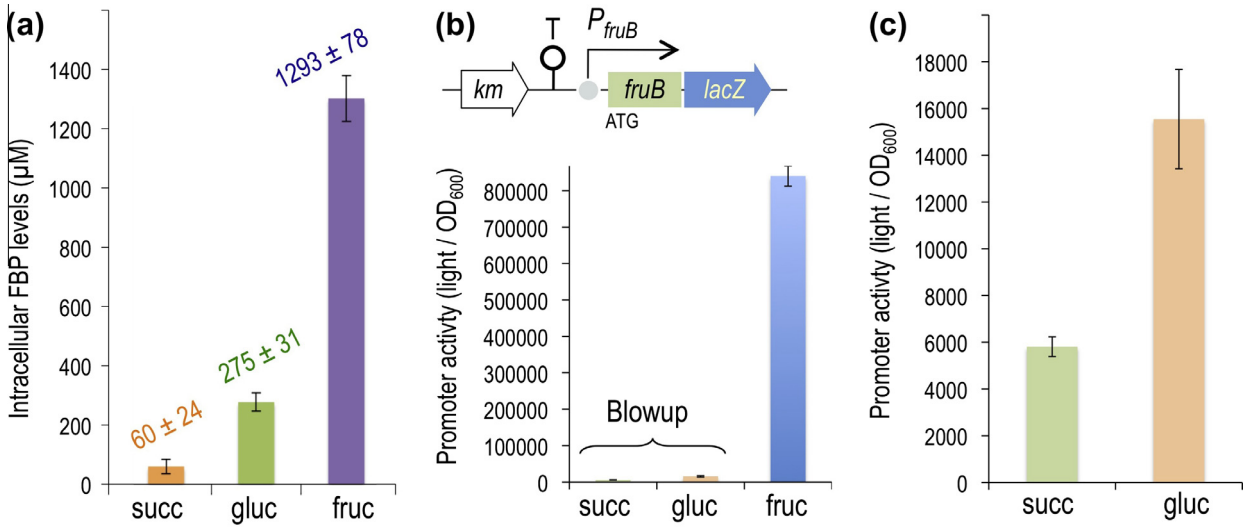

Fig. 5. Metabolic control of P_{fruB} activity. (a) FBP levels in *P. putida* growing on glycolytic (fructose and glucose) and gluconeogenic (succinate) substrates. Wild-type cells of *P. putida* KT2440 were grown in M9 media with the substrate indicated until the mid-exponential phase and then processed for measuring FBP levels by HPLC-MS as described in the Section 4. The data shown correspond to three independent samples, the error bars representing the standard deviations of the mean. (b) P_{fruB} activity in cells grown on succinate, glucose and fructose as the sole C source. A schematic diagram of the *fruB′-′lacZ* gene fusion borne by reporter plasmid pMCH1 is sketched on top. Note the very high activity in cells grown on fructose in contrast with those in succinate or glucose. (c) Blowup of *lacZ* readout of *P. putida* (pMCH1) cells growing on succinate or glucose.

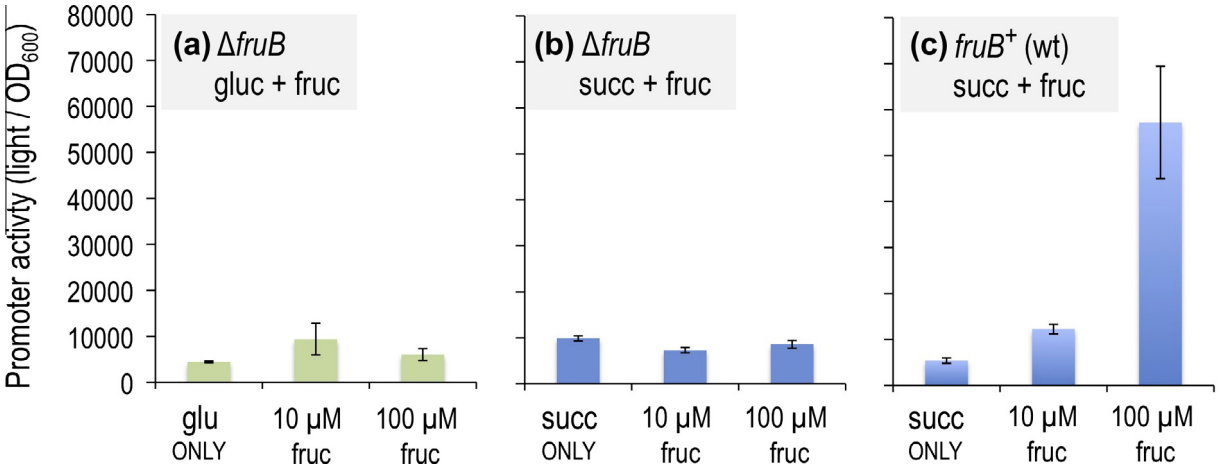

Fig. 6. Effect of Δ*fruB* on the activity of a *fruB′-′lacZ* fusion. P_{fruB} activity in *P. putida* (pMCH1) cells lacking the *fruB* gene growing in (a) glucose with increasing concentrations (10 and 100 μM) of fructose and (b) succinate with increasing concentrations (10 and 100 μM) of fructose. (c) P_{fruB} activity in wild type cells grown with succinate plus fructose. β-Galactosidase activity was measured with Galacton-Plus® as described in the Section 4. Note that *lacZ* levels of the Δ*fruB* strain remain unchanged regardless of succinate or glucose, plausibly due to the inability of cells to internalize fructose and thus generate F1P.

to the *E. coli*'s counterpart. The higher binding promiscuity of Cra^{EC} is further supported by significantly larger number of possible binding modes of both docked effectors as well as lower probability of their calculated binding modes.

2.5. Molecular dynamics of F1P and FBP bound to Cra^{PP}

To gain a further insight on the selectivity of Cra^{PP} for its physiological effector we run simulations of the interactions of F1P and FBP bound to the Cra^{PP} structure (PDB: 3O75) and the Cra^{EC} (PDB: 2IKS). Once reaching a constant temperature, the dynamically simulated systems were found to be equilibrated based on the stable values of energies, density, gyration radius and the mean root square deviation of protein backbone atoms, over the entire length of the production molecular dynamics simulation (data not show). The binding free energy calculated by MM-PBSA and the normal mode analysis for all four investigated complexes are shown in Supplementary Table S7. In good agreement with the data of docking calculations presented above, the favorable free binding energies confirm that both F1P and FBP can bind to either Cra variant. However, the divergence between the free binding energy of F1P and FBP (Supplementary Table S7) is significantly larger in the case of Cra^{PP} (−7.2 ± 2.5 kcal/mol) than *E. coli*'s Cra^{EC} (−3.8 ± 1.1 kcal/mol). Such differences imply a difference of six orders of magnitude in the affinity of Cra^{PP} for each of the effectors as compared to the 3 orders of magnitude in the case of Cra^{EC}. These analyses both account for the extreme selectivity of Cra^{PP} towards F1P and explain why the *E. coli*'s protein has, otherwise, a broader effector range *in vivo* that reaches out physiological fluctuations of FBP [13].

3. Conclusions

Inspection of the crystal structure of Cra^{PP} [16] along with the suite of biochemical and biophysical tests presented in this work reveal without a doubt, that F1P is the one and only metabolic

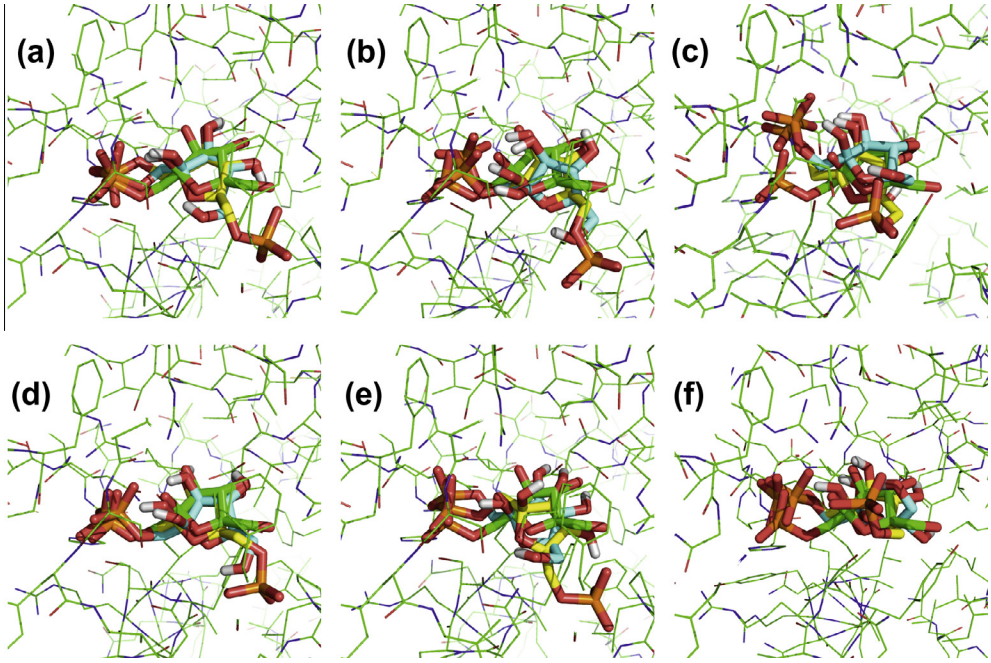

Fig. 7. Binding modes of F1P and FBP exposed by molecular docking of the effector molecules to the crystal structures of Cra^{PP} and Cra^{EC}. Predicted binding modes of F1P (cyan sticks) and FBP (yellow sticks) obtained from docking into (a) chain A of Cra^{PP} complexed with F1P (structure PDB: 3O75), (b) chain A of effector-free Cra^{PP} (structure PDB: 3O74), (c) chain A of effector-free Cra^{EC} (structure PDB: 2IKS), (d) chain B of Cra^{PP} complexed with F1P (structure PDB: 3O75), (e) chain B of effector-free Cra^{PP} (structure PDB: 3O74) and (f) chain B of effector-free Cra^{EC} (structure PDB: 2IKS). The experimentally determined conformation of F1P is shown with green sticks and the protein structures with green lines.

physiological effector of the ortholog TF that is native of *P. putida*. This is in contrast with the situation for the enterobacterial counterpart where FBP is one of the physiological agonists of the regulator. Since FBP is a key metabolite of the standard Ebmden–Meyerhoff–Parnas (EMP) pathway, its levels are considered a proxy of the glycolytic course and Cra^{EC} a flux sensor [13]. In contrast, *P. putida* lacks the EMP route and intracellular FBP concentrations are not sufficient to elicit de-repression of the P_{fruB} promoter. Moreover, according to current metabolic models for this microorganism, F1P is formed *in vivo* only as a result of fructose phosphorylation by the PTS^{Fru} system (Supplementary Fig. S1; [15,17]). Since the *P. putida*'s genome contains ⩾50 Cra boxes with the potential to control a suite of cellular functions (Supplementary Table S8), we suggest that fructose is an important environmental signal for this bacterium beyond its mere status of being a C source, an issue that deserves further studies. In any case, it seems clear that Cra (i) is used in different bacteria for sensing dissimilar physiological conditions and that (ii) such functional reassignment can be brought about by subtle modifications of its binding parameters to possible effectors. In our case, it is likely that otherwise orthologous Cra versions have been co-opted in different hosts to regulate target genes in response to unlike metabolic inputs. Such a regulatory exaptation [26] thus provides a rationale of how both TFs and their cognate regulons can dramatically diversify in different bacteria.

4. Materials and methods

4.1. Bacterial strains, plasmids, culture media, and growth conditions

All *P. putida* strains were derived from *P. putida* KT2440 [27]. Δ*fruB* strain was reported previously [17] and was constructed using de protocol described by Martínez-García et al. [28]. *P. putida* and *E. coli* strains were cultured at 30 °C and 37 °C, respectively, in an aerated orbital shaker at 170 rpm. The rich medium used to grow all strains of this study was Luria-Bertani (LB; [29]). Where indicated, *P. putida* strains were also cultured in minimal medium M9 [20], supplemented with 0.2% (w/v) fructose, glucose or succinate as the sole carbon and energy source added, if necessary with 50 μg/ml kanamycin (K_m). Broad host range pMCH1 plasmid containing a $P_{fruB} \rightarrow$ *fruB′-′lacZ* reporter translational fusion has been described previously [17]. Both plasmids were separately transformed in *P. putida* KT2440 and its Δ*fruB* variant [17] as required.

4.2. Measurements of β-galactosidase activity

The extremely sensitive Galacton-Light Plus™ system (Applied Biosystems) was employed for measuring β-galactosidase levels in *lacZ+ P. putida* cells. To this end, each strain under examination was pregrown in M9 with glucose or succinate in presence of K_m to ensure retention of the reporter plasmids and then diluted to an OD_{600} ~0.05. Once bacteria had reached OD_{600} ~0.3–0.6, the cells of 0.5 ml of each culture were spun down (2 min, 14,000×*g*) and the pellet resuspended in 200 μl of lysis buffer (100 mM potassium phosphate pH 7.8, 0.2% Triton X-100). The mixtures were subjected to two freeze-thaw cycles in liquid nitrogen and clarified by centrifugation 1 min at 14,000×*g*. 20 μl of the supernatant were then deposited in the wells of microtiter plates, added with 80 μl of reaction buffer (100 mM sodium phosphate, pH 8.0, 1 mM $MgCl_2$,

Table 1
Properties of the calculated binding modes of metabolic effectors averaged over both Cra protein chains.

Effector	Cra structure	Mean docked energy (kcal/mol)	Occurrence of binding mode (%)
F1P	3O75	−8.29	39
	3O74	−7.40	8
	2IKS	−5.65	2
FBP	3O75	−6.45	13
	3O74	−5.35	11
	2IKS	−4.72	1

F1P, fructose 1-phosphate; FBP, fructose 1,6-bisphosphate; 2IKS, effector-free Cra^{EC}; 3O74, effector-free Cra^{PP}; 3O75, Cra^{PP} complexed with F1P.

1X Galacton-Plus®) and incubated for 30 min. Samples were then added with 125 µl of Accelerator-II Sapphire-II™ and light emission recorded for 30 s in a luminometer following the instructions of the commercial supplier. All the enzymatic measurements presented through this paper are the result of at least six biological replicates.

4.3. Gel retardation assays

The P^{PP}_{fruB} probe used for these tests containing a single Cra binding site was amplified from plasmid pMCH1 with oligonucleotides 5′PfruB (5′CGAATTTTCCTTGTTATTACCGGG3′) and 3′PfruB (5′CGGAATTCGACCTTCTCCTTTTGCAGTTCCC3′, an engineered EcoRI site is underlined). The equivalent P^{EC}_{fruB} probe with two Cra binding sites was similarly amplified from the purified genomic DNA of *E. coli* W3110 by using oligonucleotides 5′PfruBcoli (5′ CTGA TA ACG GATTTTCCCATCAGC3′) and 3′PfruBcoli (5′CGGAATTCGCCTCTT CTTTGTCTCCGGCC3′; the *Eco*RI site underlined). In both cases, the amplified DNA was digested with EcoRI and the resulting 290 bp fragments were 3′-end labelled by filling-in the *Eco*RI-digested overhanging end of the fragment with [α-^{32}P]dATP and the Klenow fragment of *E. coli* DNA polymerase as reported previously [30]. The retardation reactions were set in TRRG buffer (20 mM Tris/HCl, pH 7.5, 10% glycerol, 2 mM β-mercaptoethanol and 50 mM KCl) and contained 0.05 nM DNA probe, 250 µg/ml BSA, 50 nM purified His$_6$-Cra protein (produced as described in [16]) and concentrations 1–15 mM of effectors in a final volume of 9 µl. After incubation of the retardation mixtures for 20 min at room temperature, the mixtures were analyzed by electrophoresis in 5% polyacrylamide gels buffered with 0.5X TBE (45 mM Tris/borate, 1 mM EDTA). The gels were dried on Whatman 3MM paper and exposed to X-Ray Film (Konica Minolta).

4.4. Isothermal titration microcalorimetry (ITC)

ITC experiments were performed on a VP microcalorimeter (MicroCal, Northampton, MA, USA) at 25 °C. Prior to experiments, Cra was thoroughly dialyzed in 25 mM Tris-HCl, 50 mM NaCl, 1 mM DTT, pH 8.0. After the protein solution was then clarified trough a 0.45 µm filter and its concentration was determined by UV absorption spectroscopy using and extinction coefficient of $1.217 \times 10^5\ cm^{-1}\ M^{-1}$ at 280 nm [31]. Effectors were prepared by diluting pure powdered products in filtered dialysis buffer so that the ligand and protein solvent were the same. Titration with F1P (positive control) involved 4.8 µl injections of 0.5 mM F1P into a 12 µM protein solution. On the other hand, titration with FBP and G6P involved 14.4 µl injections of 1 mM FBP (or G6P) into a 12 µM protein solution. For competition experiments a mixture of 5 mM of FBP with 12 µM of Cra protein was titrated with a mixture of 0.45 µM of F1P and 5 mM of FBP. For all the experiments, the mean enthalpies measured from injection of the ligands into the buffer were subtracted from raw titration data prior to data fitting using the *One binding site model* of the MicroCal version of the ORIGIN software. From the curves thus fitted, the parameters ΔH (reaction enthalpy), K_A (binding constant, $K_A = 1/K_D$), and n (reaction stoichiometry) were determined. From the values of K_A and ΔH, the change in free energy (ΔG) and in entropy (ΔS) were calculated with the equation: $\Delta G = -RT \ln K_A = \Delta H - T\Delta S$, where R is the universal molar gas constant and T is the absolute temperature.

4.5. Determination of FBP concentrations by liquid chromatography mass spectrometry

For quantification of FBP, *P. putida* KT2440 were pregrown in M9 medium with 0.2% (w/v) fructose, glucose or succinate as required and then re-inoculated in the same media to a starting OD_{600} = 0.05. Cultures were then let grow until exponential phase, at which point the biomass corresponding to 0.5–0.6 mg of cellular dry weight (CDW, 4 ml of culture to OD_{600} ~0.5–0.6) of triplicate samples was collected by fast centrifugation (13,000×*g*, 30 sec) and the bacterial pellets immediately frozen in liquid nitrogen until further processing. At that point, samples were extracted three times with 0.5 ml 60% (v/v) ethanol buffered with 10 mM ammonium acetate pH 7.2 at 78 °C for 1 min as described previously [32,33]. After each extraction step, biomass was separated by centrifugation for 1 min at 13,000×*g*. The three liquid extracts of each sample were pooled prior to drying at 120 µbar to complete dryness and then stored at −80 °C. Samples were then resuspended in 20 µl of MilliQ water, sealed in 96-well plates, submitted to LC-MS and the data analyzed as described previously [33].

4.6. Molecular docking calculations

The molecular models of F1P and FBP were prepared and energy-minimized in the Avogadro 1.0.2 package [34]. The procedure involved 500 steps of steepest descent followed by 500 steps of conjugate gradient using the GAFF force field [35]. The crystal structures were downloaded from RSCB PDB database under following PDB codes: 2IKS (effector-free Cra from *E. coli*), 3O74 (effector-free Cra from *P. putida*), and 3O75 (Cra from *P. putida* complexed with F1P). All crystallographic water molecules were removed and hydrogen atoms were added to the proteins by H++ server at pH 8.0 using the default settings [36]. Gasteiger charges and AutoDock 4.2 atom types were assigned to protein and ligand structures by MGLTools [37]. During docking procedure, the receptor binding site was represented by the set of atomic and electrostatic grid maps calculated by AutoGrid 4.2 [38,39]. Individual chains of Cra structures were aligned to the chain A of 3O74 structure using Pymol 1.4.1 (http://pymol-molecular-graphics-system.soft112.com) and the grid maps were set to $80 \times 80 \times 80$ grid points with spacing 0.25 Å centered at the position of C2 atom of F1P bound to chain A of 3O75. This setting of the grid maps allows full coverage of Cra binding site. Both ligands were then docked separately into the binding sites of each chain of all structures using AutoDock 4.2 [38,39]. 250 docking calculations were performed for each ligand employing the Lamarckian Genetic algorithm with the following parameters: initial population size 300, maximum of 30,000 generations, elitism value 1, mutation rate 0.02, and cross-over rate 0.8. The maximum of energy evaluations were set to 10,000,000. The local search was based on pseudo Solis and Wets algorithm with a maximum of 300 iterations per local search [40]. Energy of unbound system was estimated as the internal energy of the unbound extended conformation determined from Lamarckian Genetic Algorithm search. Final orientations from every docking run were clustered with a clustering tolerance for the root-mean-square positional deviation of 1.5 Å.

4.7. Molecular dynamics simulations

The F1P-3O75, FBP-3O75, F1P-2IKS and FBP-2IKS complexes obtained by the molecular docking were used as the initial structures for the molecular dynamics simulations. Crystallographic waters were put back to their original positions with the exception of water molecules overlapping with the docked effectors. AM1-BCC atomic partial charges [41] and the force field parameters for F1P and FBP were generated with the Antechamber module of AMBER11 [42,43] using the total charges of −2 e and −4 e for F1P and FBP, respectively. Using Tleap module of AMBER11, the systems were neutralized by adding 8, 10, 16 and 18 Na^+ ions to F1P-3O75, FBP-3O75, F1P-2IKS and FBP-2IKS complexes, respectively. Using the same module, an octahedral of TIP3P water molecules [44] was added to the distance of 10 Å from any solute

atom in the systems. Energy minimization and molecular dynamics simulations were carried out in PMEMD module of AMBER11 using ff99SB force field [45] for a protein and GAFF force field [35] for the ligands. Initially, the investigated systems were minimized by 500 steps of steepest descent followed by 500 steps of conjugate gradient in five rounds of decreasing harmonic restraints. The restraints were applied as follows: 500 kcal mol^{-1} $Å^{-2}$ on all heavy atoms of a protein, and then 500, 125, 25 and 0 kcal mol^{-1} $Å^{-2}$ on the backbone atoms only. Molecular dynamics simulations employed periodic boundary conditions, the particle mesh Ewald method for treatment of the electrostatic interactions [46,47], 10 Å cutoff for nonbonded interactions, and 2 ft time step with the SHAKE algorithm to fix all bonds containing hydrogens [48]. Equilibration simulations consisted of two steps: (i) 20 ps of gradual heating from 0 to 300 K under constant volume, using a Langevin thermostat with collision frequency of 1.0 ps^{-1}, and with harmonic restraints of 5.0 kcal mol^{-1} $Å^{-2}$ on the position of all protein and effector atoms, and (ii) 2000 ps of unrestrained molecular dynamics at 300 K using the Langevin thermostat, and constant pressure of 1.0 bar using pressure coupling constant of 1.0 ps. Finally, production molecular dynamics simulations were run for 10 ns with the same settings as the second step of equilibration simulations. Coordinates were saved in 1 ps interval, and the trajectories were analyzed using Ptraj module of AMBER11, and visualized in Pymol 1.4.1 (see above) and VMD 1.8.9 [49].

4.8. Calculation of the binding free energy

The free energy for the binding of potential effectors to the individual proteins was calculated by the Molecular Mechanics/Poisson Boltzmann Surface Area (MM-PBSA) method using *MMPBSA.py* script of AMBER11 [50]. The polar solvation free energy contributions were determined by grid based finite-difference solution of the Possion–Boltzmann equation using *pbsa* [51] program of AMBER11 The setting of the Possion–Boltzmann calculations were following: ionic strength of 75 mM, grid spacing of 0.5 Å, the internal and external dielectric constants of 1 and 80, respectively, and modified Bondi radii [52] for ligands. The nonpolar solvation free energy contribution was estimated as proportional to the solvent accessible surface area using the LCPO method [53]. The entropy change upon effector binding was evaluated using the normal-mode analysis implemented in NAB module of AMBER11 using distance-dependent dielectric of $4r_{ij}$. The energy was calculated over 10,000 snapshots extracted from a single production molecular dynamics simulation of a complex, and the entropy contribution was calculated from 100 snapshots evenly sampled from the snapshots employed in the energy calculation.

Acknowledgements

Authors are indebted to Tobias Führer and Uwe Sauer (ETH Zürich) for help with measurements of central metabolites. This study was supported by the BIO and FEDER CONSOLIDER-INGENIO programme of the Spanish Ministry of Science and Innovation, the MICROME, ST-FLOW and ARISYS Contracts of the EU, the PROMT Project of the CAM, the European Regional Development Fund (CZ.1.05/2.1.00/01.0001) and the Grant Agency of the Czech Republic (P503/12/0572). CERIT-SC and MetaCentrum are acknowledged for providing access to their computing facilities (CZ.1.05/3.2.00/08.0144 and LM2010005). J.B. was supported by the CZ1.07/2.3.00/30.0037 Program of the European Social Fund and the Czech Republic. Authors declare no conflict of interest.

Appendix A. Supplementary data

Supplementary data associated with this article can be found, in the online version, at http://dx.doi.org/10.1016/j.fob.2014.03.013.

References

[1] Saier Jr., M.H. and Ramseier, T.M. (1996) The catabolite repressor/activator (Cra) protein of enteric bacteria. J. Bacteriol. 178, 3411–3417.
[2] Ramseier, T.M. (1996) Cra and the control of carbon flux via metabolic pathways. Res. Microbiol. 147, 489–493.
[3] Ow, D.S., Lee, R.M., Nissom, P.M., Philp, R., Oh, S.K. and Yap, M.G. (2007) Inactivating FruR global regulator in plasmid-bearing *Escherichia coli* alters metabolic gene expression and improves growth rate. J. Biotechnol. 131, 261–269.
[4] Bledig, S.A., Ramseier, T.M. and Saier Jr., M.H. (1996) FruR mediates catabolite activation of pyruvate kinase (*pykF*) gene expression in *Escherichia coli*. J. Bacteriol. 178, 280–283.
[5] Sarkar, D., Siddiquee, K.A., Arauzo-Bravo, M.J., Oba, T. and Shimizu, K. (2008) Effect of *cra* gene knockout together with edd and *iclR* genes knockout on the metabolism in *Escherichia coli*. Arch. Microbiol. 190, 559–571.
[6] Geerse, R.H., van der Pluijm, J. and Postma, P.W. (1989) The repressor of the PEP:fructose phosphotransferase system is required for the transcription of the pps gene of *Escherichia coli*. Mol. Gen. Genet. 218, 348–352.
[7] Negre, D., Oudot, C., Prost, J.F., Murakami, K., Ishihama, A., Cozzone, A.J. and Cortay, J.C. (1998) FruR-mediated transcriptional activation at the ppsA promoter of *Escherichia coli*. J. Mol. Biol. 276, 355–365.
[8] Cortay, J.C., Negre, D., Scarabel, M., Ramseier, T.M., Vartak, N.B., Reizer, J., Saier Jr., M.H. and Cozzone, A.J. (1994) In vitro asymmetric binding of the pleiotropic regulatory protein, FruR, to the *ace* operator controlling glyoxylate shunt enzyme synthesis. J. Biol. Chem. 269, 14885–14891.
[9] Prost, J.F., Negre, D., Oudot, C., Murakami, K., Ishihama, A., Cozzone, A.J. and Cortay, J.C. (1999) Cra-dependent transcriptional activation of the *icd* gene of *Escherichia coli*. J. Bacteriol. 181, 893–898.
[10] Ramseier, T.M., Chien, S.Y. and Saier Jr., M.H. (1996) Cooperative interaction between Cra and Fnr in the regulation of the *cydAB* operon of *Escherichia coli*. Curr. Microbiol. 33, 270–274.
[11] Ramseier, T.M., Negre, D., Cortay, J.C., Scarabel, M., Cozzone, A.J. and Saier Jr., M.H. (1993) In vitro binding of the pleiotropic transcriptional regulatory protein, FruR, to the *fru*, *pps*, *ace*, *pts* and *icd* operons of *Escherichia coli* and *Salmonella typhimurium*. J. Mol. Biol. 234, 28–44.
[12] Ramseier, T.M., Bledig, S., Michotey, V., Feghali, R. and Saier Jr., M.H. (1995) The global regulatory protein FruR modulates the direction of carbon flow in *Escherichia coli*. Mol. Microbiol. 16, 1157–1169.
[13] Kotte, O., Zaugg, J.B. and Heinemann, M. (2010) Bacterial adaptation through distributed sensing of metabolic fluxes. Mol. Sys. Biol. 6, 355.
[14] Kochanowski, K., Volkmer, B., Gerosa, L., Haverkorn van Rijsewijk, B.R., Schmidt, A. and Heinemann, M. (2013) Functioning of a metabolic flux sensor in *Escherichia coli*. Proc. Natl. Acad. Sci. USA 110, 1130–1135.
[15] Chavarria, M., Kleijn, R.J., Sauer, U., Pfluger-Grau, K., Casasnovas, J.M. and de Lorenzo, V. (2012) Regulatory tasks of the phosphoenolpyruvate-phosphotransferase system of *Pseudomonas putida* in central carbon metabolism. mBio 3. e00028–00012.
[16] Chavarria, M., Santiago, C., Platero, R., Krell, T., Casasnovas, J.M. and de Lorenzo, V. (2011) Fructose 1-phosphate is the preferred effector of the metabolic regulator Cra of *Pseudomonas putida*. J. Biol. Chem. 286, 9351–9359.
[17] Chavarria, M., Fuhrer, T., Sauer, U., Pfluger-Grau, K. and de Lorenzo, V. (2013) Cra regulates the cross-talk between the two branches of the phosphoenolpyruvate: phosphotransferase system of *Pseudomonas putida*. Environ. Microbiol. 15, 121–132.
[18] Bennett, B.D., Kimball, E.H., Gao, M., Osterhout, R., Van Dien, S.J. and Rabinowitz, J.D. (2009) Absolute metabolite concentrations and implied enzyme active site occupancy in *Escherichia coli*. Nat. Chem. Biol. 5, 593–599.
[19] Silva-Rocha, R. and de Lorenzo, V. (2012) Broadening the signal specificity of prokaryotic promoters by modifying cis-regulatory elements associated with a single transcription factor. Mol. BioSys. 8, 1950–1957.
[20] Miller, J.H. (1972) Experiments in molecular genetics, Cold Spring Harbor, N.Y.
[21] Jain, V.K. and Magrath, I.T. (1991) A chemiluminescent assay for quantitation of beta-galactosidase in the femtogram range: application to quantitation of beta-galactosidase in *lacZ*-transfected cells. Anal. Biochem. 199, 119–124.
[22] Nogales, J., Palsson, B.O. and Thiele, I. (2008) A genome-scale metabolic reconstruction of *Pseudomonas putida* KT2440: iJN746 as a cell factory. BMC Syst. Biol. 2, 79.
[23] Puchalka, J., Oberhardt, M.A., Godinho, M., Bielecka, A., Regenhardt, D., Timmis, K.N., Papin, J.A. and Martins dos Santos, V.A. (2008) Genome-scale reconstruction and analysis of the *Pseudomonas putida* KT2440 metabolic network facilitates applications in biotechnology. PLoS Comput. Biol. 4, e1000210.
[24] McMurry, J.E. and Begley, T.P. (2005) The organic chemistry of biological pathways, Roberts and Company Publishers, Colorado.
[25] Wrolstad, R.E. (2012) Food Carbohydrate Chemistry, John Wiley & Sons Inc, West Sussex, UK.

[26] Milanesio, P., Arce-Rodriguez, A., Munoz, A., Calles, B. and de Lorenzo, V. (2011) Regulatory exaptation of the catabolite repression protein (Crp)-cAMP system in *Pseudomonas putida*. Environ. Microbiol. 13, 324–339.
[27] Nelson, K.E., Weinel, C., Paulsen, I.T., Dodson, R.J., Hilbert, H., Martins dos Santos, V.A., Fouts, D.E., Gill, S.R., Pop, M., Holmes, M., Brinkac, L., Beanan, M., DeBoy, R.T., Daugherty, S., Kolonay, J., Madupu, R., Nelson, W., White, O., Peterson, J., Khouri, H., Hance, I., Chris Lee, P., Holtzapple, E., Scanlan, D., Tran, K., Moazzez, A., Utterback, T., Rizzo, M., Lee, K., Kosack, D., Moestl, D., Wedler, H., Lauber, J., Stjepandic, D., Hoheisel, J., Straetz, M., Heim, S., Kiewitz, C., Eisen, J.A., Timmis, K.N., Dusterhoft, A., Tummler, B. and Fraser, C.M. (2002) Complete genome sequence and comparative analysis of the metabolically versatile *Pseudomonas putida* KT2440. Environ. Microbiol. 4, 799–808.
[28] Martinez-Garcia, E. and de Lorenzo, V. (2011) Engineering multiple genomic deletions in Gram-negative bacteria: analysis of the multi-resistant antibiotic profile of *Pseudomonas putida* KT2440. Environ. Microbiol. 13, 2702–2716.
[29] Sambrook, J., Maniatis, T. and Fritsch, T. (1989) Molecular cloning: a laboratory manual, Cold Spring Harbor Laboratory Press, N.Y..
[30] Barragan, M.J., Blazquez, B., Zamarro, M.T., Mancheno, J.M., Garcia, J.L., Diaz, E. and Carmona, M. (2005) BzdR, a repressor that controls the anaerobic catabolism of benzoate in *Azoarcus* sp. CIB, is the first member of a new subfamily of transcriptional regulators. J. Biol. Chem. 280, 10683–10694.
[31] Gasteiger, E., Hoogland, C., Gattiker, A., Duvaud, S., Wilkins, M.R., Appel, R.D. and Bairoch, A. (2005) Protein Identification and Analysis Tools on the ExPASy Server in: The Poteomics Protocols Handbook (Walker, J.M., Ed.), pp. 571–607, Humana Press.
[32] Fuhrer, T. and Sauer, U. (2009) Different biochemical mechanisms ensure network-wide balancing of reducing equivalents in microbial metabolism. J. Bacteriol. 191, 2112–2121.
[33] Buescher, J.M., Moco, S., Sauer, U. and Zamboni, N. (2010) Ultrahigh performance liquid chromatography-tandem mass spectrometry method for fast and robust quantification of anionic and aromatic metabolites. Anal. Chem. 82, 4403–4412.
[34] Hanwell, M.D., Curtis, D.E., Lonie, D.C., Vandermeersch, T., Zurek, E. and Hutchison, G.R. (2012) Avogadro: an advanced semantic chemical editor, visualization, and analysis platform. J. Cheminform. 4, 17.
[35] Wang, J., Wolf, R.M., Caldwell, J.W., Kollman, P.A. and Case, D.A. (2004) Development and testing of a general amber force field. J. Comput. Chem. 25, 1157–1174.
[36] Gordon, J.C., Myers, J.B., Folta, T., Shoja, V., Heath, L.S. and Onufriev, A. (2005) H++: a server for estimating pKas and adding missing hydrogens to macromolecules. Nucl. Acids Res. 33, W368–W371.
[37] Sanner, M.F. (1999) Python: a programming language for software integration and development. J. Mol. Graph. Model. 17, 57–61.
[38] Morris, G.M., Goodsell, D.S., Halliday, R.S., Huey, R., Hart, W.E., Belew, R.K. and Olson, A.J. (1998) Automated docking using a Lamarckian genetic algorithm and an emperical binding free energy function. J. Comput. Chem. 19, 1639–1662.
[39] Huey, R., Morris, G.M., Olson, A.J. and Goodsell, D.S. (2007) A semiempirical free energy force field with charge-based desolvation. J. Comput. Chem. 28, 1145–1152.
[40] Solis, F.J. and Wets, R.J.B. (1981) Minimization by random search techniques. Math. Oper. Res. 6, 19–30.
[41] Jakalian, A., Bush, B.L., Jack, D.B. and Bayly, C.I. (2000) Fast, efficient generation of high-quality atomic charges. AM1-BCC model: I. Method. J. Comput. Chem. 21, 132–146.
[42] Case, D.A., Darden, T.A., Cheatham, T.E., Simmerling, C.L., Wang, J., Duke, R.E., Luo, R., Walker, R.C., Zhang, W., Merz, K.M., Roberts, B., Wang, B., Hayik, S., Roitberg, A., Seabra, G., Kolossváry, I., Wong, K.F., Paesani, F., Vanicek, J., Wu, X., Brozell, S.R., Steinbrecher, T., Gohlke, H., Cai, Q., Ye, X., Wang, J., Hsieh, M.J., Cui, G., Roe, D.R., Mathews, D.H., Seetin, M.G., Sagui, C., Babin, V., Luchko, T., Gusarov, S., Kovalenko, A. and Kollman, P.A. (2010) AMBER 11 in, University of California, San Francisco.
[43] Case, D.A., Cheatham, T.E., Darden, T., Gohlke, H., Luo, R., Merz, K.M., Onufriev, A., Simmerling, C., Wang, B. and Woods, R.J. (2005) The Amber biomolecular simulation programs. J. Comput. Chem. 26, 1668–1688.
[44] Jorgensen, W.L., Chandrasekhar, J., Madura, J.D., Impey, R.W. and Klein, M.L. (1983) Comparison of simple potential functions for simulating liquid water. J. Chem. Phys. 79, 926–935.
[45] Hornak, V., Abel, R., Okur, A., Strockbine, B., Roitberg, A. and Simmerling, C. (2006) Comparison of multiple Amber force fields and development of improved protein backbone parameters. Proteins 65, 712–725.
[46] Darden, T., York, D. and Pedersen, L. (1993) Particle mesh Ewald: an N log(N) method for Ewald sums in large systems. J. Chem. Phys. 103, 8577–8593.
[47] Essmann, U., Perera, L., Berkowitz, M., Darden, T., Lee, H. and Pedersen, L. (1995) A smooth particle mesh Ewald method. J. Chem. Phys. 103, 8577–8593.
[48] Ryckaert, J.P., Ciccotto, G. and Berendsen, H.J.C. (1977) Numerical integration of the cartesian equations of motion of a system with constraints: molecular dynamics of *n*-alkanes. J. Comput. Phys. 23, 327–341.
[49] Humphrey, W., Dalke, A. and Schulten, K. (1996) VMD: visual molecular dynamics. J. Mol. Graph. 14, 33–38.
[50] Srinivasan, J., Cheatham, T.E., Cieplak, P., Kollman, P.A. and Case, D.A. (1998) Continuum solvent studies of the stability of DNA, RNA, and phosphoramidate−DNA helices. J. Am. Chem. Soc. 120, 9401–9409.
[51] Luo, R., David, L. and Gilson, M.K. (2002) Accelerated Poisson–Boltzmann calculations for static and dynamic systems. J. Comput. Chem. 23, 1244–1253.
[52] Onufriev, A., Bashford, D. and Case, D.A. (2004) Exploring protein native states and large-scale conformational changes with a modified generalized born model. Proteins 55, 383–394.
[53] Weiser, J., Shenkin, P. and Still, C. (1999) Approximate atomic surfaces from linear combinations of pairwise overlaps (LCPO). J. Comput. Chem. 20, 217–230.